Aerodynamics of Complex Bodies of Revolution

Veysel Atli*
Istanbul Technical University, Istanbul, Turkey

The aerodynamics of five complex bodies of revolution are investigated experimentally and theoretically at a low Mach number ($M_\infty \cong 0.1$) and over the range of angle of attack from 0 to 35 deg. The geometrical forms of the bodies are generally complex with the discontinuities in the slope of the body surface. The surface-flow visualization is performed by using the oil method. The balance measurements were made and the results compared with the potential theory and the method based on the crossflow analogy. It was observed that the discontinuities in the slope of the body surface make the flow separation and consequently the flowfield very complicated. It was also found that the method of crossflow analogy is applicable not only to simple-type bodies of revolution but also the complex ones.

Nomenclature

C_A = axial force coefficient
C_D = drag coefficient
C_{Do} = drag coefficient at $\alpha = 0$ deg
C_d = crossflow drag coefficient
c_{dc} = crossflow drag coefficient of circular cylinder section
C_L = lift coefficient
C_M = pitching moment coefficient
d = maximum body diameter
d_s = diameter of corresponding cylinder to body of revolution ($= S_p/l$)
$f(x)$ = normal force distribution
l = total body length
l_r = reference length
M_∞ = freestream Mach number
M_{c_∞} = crossflow Mach number ($= M_\infty \sin\alpha$)
q_∞ = freestream dynamic pressure ($q_\infty = \frac{1}{2}\rho V_\infty^2$)
R = local body radius
Re_d = Reynolds number based on the maximum body diameter d ($Re_d = V_\infty d/\upsilon$)
Re_{cd_s} = crossflow Reynolds number based on d_s ($= V_\infty \sin\alpha\, ds/\upsilon$)
Re_l = Reynolds number based on l
S = local cross-sectional area ($= \pi R^2$)
S_b = body base area
S_p = body planform area ($= \int_0^l 2R\, dx$)
S_r = reference area
S_t = body flat-nose area
V_∞ = freestream velocity
W = body volume ($= \int_0^l \pi R^2\, dx$)
x = body axis (axial distance from body nose)
x_c = axial distance from body nose to centroid of body planform area
x_{cp} = axial distance from body nose to center of pressure
x_m = pitching moment center (axial distance from body nose to pitching moment center)
α = angle of attack
ρ = density of air
υ = kinematic viscosity of air
η = correction factor for influence of fineness ratio on c_{dc}

Received Dec. 19, 1986; revision received June 25, 1987.

*Assistant Professor, Faculty of Aeronautics and Astronautics.

Introduction

THE flowfield around, and, consequently, the aerodynamic characteristics of a missile-type body of revolution, depend on the geometrical form of the body, angle of attack, Mach number, and Reynolds number. At an angle of attack greater than a few degrees, because of the viscosity, the flow around even a simple-type body of revolution (the radius of the body R is a monotonic function of the body axis x, such as a tangent ogive body) separates from the lee side of the body and rolls up to form vortices in the leeward flowfield. This large-scale leeward flow separation produces a large increase in the normal force distribution reducing the lee-side pressure. The variations of the aerodynamic loads with the angle of attack become nonlinear. Although the potential theory is sufficient at small angles of attack, it is necessary to consider the effects of the leeward flow separation at high angles of attack. For this purpose, some certain theoretical, semi-empirical and empirical methods have already been developed.[1] Unfortunately, the theoretical and semi-empirical methods have large computational requirements and tend to be restricted to subsonic flows.[1] In the viscous crossflow analogy that is an empirical method, an empirical term representing the viscous leeward flow separation is added to a term representing potential theory for the normal force and pitching moment. This relatively simple method was originally proposed by Allen[2,3] and has successfully been applied to the simple-type bodies of revolution in many studies.[3-14] The comparison of this method with the available experimental data for the simple-type bodies of revolution has shown a good agreement not only at small angles of attack but also at high angles of attack.[8,10,13,14] Obviously, if the geometrical form of the body of revolution is complex with the discontinuities in the slope of the body surface, having junctions, gaps and flat nose, the flowfield around the body becomes much more complex than that around a simple-type body of revolution. This is because the flow separation in this case is caused not only by the angle of attack but also by the discontinuities on the surface of the body.

There are already many experimental and theoretical studies performed on the missile aerodynamics. References 15–18 represent only a few of the recent ones. Wardlaw,[1] Nielsen,[19] and Esch[20] give many more references in their studies in which the available predictive methods and experimental techniques are also reviewed. However, these studies are generally devoted to the simple-type missile bodies such as tangent ogive body, sharp cone cylinder, etc. In practice, the complex-type bodies of revolution with junctions, gaps, and flat nose are also used for missiles because, in many cases, the form of a missile is given not only by the aerodynamic requirements but also by the payload, warhead, etc. In fact, the new demands to improve performance and maneuverability of missiles make it necessary

to perform new experimental and theoretical researches by using different configurations over the wide ranges of parameters.

In the present work, the aerodynamics of five different complex-type bodies of revolution were investigated experimentally and theoretically at the Mach number $M_\infty \cong 0.1$ and the Reynolds number based on the maximum diameter of the body $Re_d \cong 1 \times 10^5$. In the experimental part of this work, first the surface flow visualization was performed by applying the oil method at the angles of attack $\alpha = 0$ and 15 deg. Hence, the flow separations on the bodies were investigated qualitatively. Then, the balance measurements were made by using a three-component mechanical balance, over the range of angle of attack $0 \leqq \alpha \leqq 35$ deg. In the theoretical part of this work, the formulation of the method based on the viscous crossflow analogy was given in a form that is applicable to the flat-nosed bodies as well as to the closed-nosed bodies. This method was, then, applied to the complex-type bodies considered here. The comparison was made between the experimental and the theoretical results for the variations of the aerodynamic characteristics with the angle of attack.

Description of the models and the experimental technique is presented in the following section. The theoretical basis and the application of the theory are next explained, followed by experimental and theoretical results, and the conclusion. A more detailed description of the current work may be found in Ref. 21.

Description of Models and Experimental Technique

The configurations of the models are presented in Fig. 1. All the models have the same fineness ratio $l/d = 7.5$, where l is the total length and d is the maximum body diameter. The geometrical forms of the models were chosen in such a way as to permit the observation of the effects of the certain geometrical differences on the flowfield and on the aerodynamic characteristics. While the first model is a constant-diameter cylinder, the last one has a geometrical shape of a particular missile with junctions, gaps, and flat nose, consisting of cylindrical and conical parts. The other models have the forms between the first and last one, so that the second one is a hemiellipsoid-cylinder, the third one a truncated cone-cylinder, and the fourth a slightly modified form of the last one.

The surface flow visualization was made by applying the oil method, in order to observe the flow separations on the bodies. These flow visualization tests were conducted in an open-circuit wind tunnel[21] with a test section of $30 \times 30 \times 100$ cm at the freestream velocity $V_\infty = 27$ m/s (i.e., the Reynolds number $Re_d = 1.25 \times 10^5$) and at the angles of attack $\alpha = 0$ and 15 deg. The photographs were taken by a camera from one side during the tunnel run.

The force and moment measurements were performed in a closed-circuit wind tunnel with a test section of $80 \times 110 \times 162$ cm by using a three-component mechanical "Merrill" balance. These measurements were made at the freestream velocity $V_\infty = 29$ m/s (i.e., $Re_d = 1.34 \times 10^5$) and over the range of angle of attack $0 \leqq \alpha \leqq 35$ deg. The measured values were corrected for the aerodynamic loads acting on the balance arms during the tests. For the balance measurements, the errors were estimated to be less than 7, 1, and 4% for normal force, pitching moment, and axial force, respectively.[21]

Theoretical Basis: The Method Based on the Viscous Crossflow Analogy

In the method based on the viscous crossflow analogy, the crossflow around an inclined slender body is treated independently from the axial flow, and the effects of the viscous leeward flow separation are considered by the viscous crossflow analogy. According to the viscous crossflow analogy, the crossflow around a slender body moving at the velocity V_∞, with the angle-of-attack α, is similar to the two-dimensional flow around a corresponding circular cylinder moving at the velocity $V_\infty \sin\alpha$.[1,3,20,21] Hence, the normal force distribution on a body of revolution of a finite length l, moving at the velocity V_∞ and the angle-of-attack α may be expressed as

$$f(x) = q_\infty \left(\frac{dS}{dx}\right) \sin 2\alpha \cos\frac{\alpha}{2} + 2\eta c_{dc}(x) R q_\infty \sin^2\alpha \qquad (1)$$

where the first term on the right-hand side comes from the potential theory and the second term is the contribution of the viscous leeward flow separation. From the Eq. (1) the normal force coefficient

$$C_N = \left[\frac{N}{q_\infty S_r} = \frac{\int_0^l f(x)\,dx}{q_\infty S_r}\right]$$

and the pitching moment coefficient about an arbitrary position an axial distance x_m from the nose

$$C_M = \left[\frac{M}{q_\infty S_r l_r} = \frac{\int_0^l f(x)\,(x_m - x)\,dx}{q_\infty S_r l_r}\right]$$

may be derived as[21]

$$C_N = \left(\frac{S_b - S_t}{S_r}\right) \sin 2\alpha \cos\frac{\alpha}{2} + C_d \frac{S_p}{S_r} \sin^2\alpha \qquad (2)$$

$$C_M = \left[\frac{W - S_b(l - x_m) - S_r x_m}{S_r l_r}\right] \sin 2\alpha \cos\frac{\alpha}{2} + C_d \frac{S_p}{S_r}\left(\frac{x_m - x_c}{l_r}\right) \sin^2\alpha \qquad (3)$$

where

$$C_d = \frac{\int_0^l \eta c_{dc}(x) 2R\,dx}{S_p} \qquad (4)$$

$$x_c = \frac{\int_0^l \eta c_{dc}(x) 2Rx\,dx}{S_p C_d} \qquad (5)$$

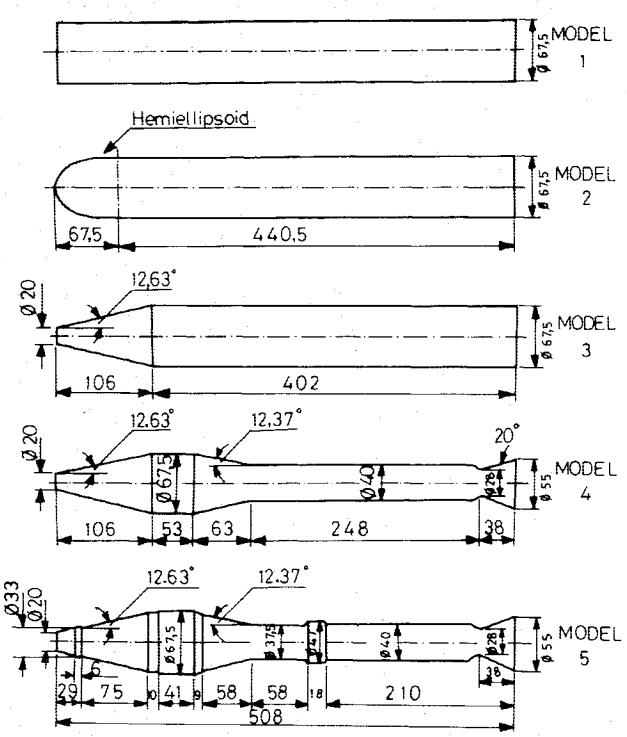

Fig. 1 Geometrical dimensions of the bodies of revolution (all dimensions in mm, scale = 1/5).

Obviously, the first terms on the right hand sides of Eqs. (2) and (3) come from the potential theory, while the second terms represent the effects of the viscous leeward flow separation. For $S_l = 0$, Eqs. (2) and (3) take the forms given in the literature[3,10–14] for the closed-nosed bodies. Therefore, Eqs. (2) and (3) may be used for the closed-nosed as well as for the flat-nosed bodies of revolution. It is obvious that C_d and x_c should be evaluated first in order to calculate C_N and C_M from Eqs. (2) and (3). For this purpose, the bodies may be tested at $\alpha = 90$ deg in the wind tunnel, as has been done by Allen and Perkins.[3] But, these parameters may also be calculated by using the available sufficient experimental drag data on cylinders in two-dimensional flow.[3] The variation of c_{dc} with the crossflow Mach number and the crossflow Reynolds number and the variation of η with ratio of length of the cylinder to diameter of the cylinder is given in Refs. 10, 13, 14, and 21, based on the experimental data. It is not easy to calculate C_d and x_c from Eqs. (4) and (5) by assuming that c_{dc} and η are functions of x. Therefore, Allen and Perkins[3] have assumed that the crossflow around a body of revolution of finite-length l moving at the velocity V_∞ and with the angle-of-attack α is similar to the crossflow around a corresponding cylinder of finite-length l and the constant diameter $d_s = S_p/l$ moving at the velocity $V_\infty \sin\alpha$. Thus, since c_{dc} and η are not functions of x, the Eqs. (4) and (5) become, respectively, as

$$C_d = nc_{dc} \tag{6}$$

$$x_c = \frac{\int_0^l 2Rx\, dx}{S_p} \tag{7}$$

where the value of c_{dc} corresponds to the crossflow Reynolds number

$$Re_{cd_s} = \left(\frac{V_\infty \sin\alpha\, d_s}{\upsilon}\right)$$

and the crossflow Mach number $M_c (= M_\infty \sin\alpha)$, while the value of η corresponds to the ratio of l/d_s. The data given in the literature[10,13,14,21] for η is for subsonic conditions, but in practice it has been found that η should be set to unit in supersonic flow.[1] Hence, C_d may be calculated from the Eq. (6) by using the experimental data given in the literature[10,13,14,21] for c_{dc} and η for the circular cylinders.

For rough engineering estimations, the axial force coefficient for slender bodies may be approximated as

$$C_A = C_{Do} \cos^2\alpha \tag{8}$$

by assuming that the axial force is produced only by the axial flowfield that is similar to the flowfield in the $\alpha = 0$ deg case.[10,13,21] Here, C_{Do} is the drag coefficient at $\alpha = 0$ deg.

After the determination of C_N, C_A, and C_M, the lift and drag coefficients and the position of the center of pressure may be obtained, respectively, by

$$C_L = C_N \cos\alpha - C_A \sin\alpha \tag{9}$$

$$C_D = C_N \sin\alpha + C_A \cos\alpha \tag{10}$$

$$\frac{x_{cp}}{l_r} = \left(\frac{x_m}{l_r} - \frac{C_M}{C_N}\right) \tag{11}$$

where x_{cp} shows the axial distance from the body nose to the center of pressure.[13,21] In the theoretical application performed here, in order to calculate C_A by using the Eq. (8), the values of C_{Do} were obtained by the balance measurements.

Results and Discussion

The surface flow visualization photographs for $\alpha = 0$ and 15 degs are shown in Fig. 2. The limiting stream lines and the separation lines on the bodies are observable from these photographs. Hence, these photographs give some qualitative results about the effects of the geometrical shape and the angle of attack on the flowfield.

The photographs for $\alpha = 0$ deg make it clear that the discontinuities in the slope of the body surface cause the circular flow separations. The separated flow from the flat nose of the model 1 reattaches to the surface at a distance of about 1.5 diameter of the cylinder from the nose, producing a circular separation bubble. Similar circular flow separations (or bubbles) that are smaller in scale are observed around the truncated conical noses of the models 3–5. The circular separation bubbles around the discontinuity between the hemiellipsoidal nose and the cylindrical part of model 2 is smaller than that around the discontinuity between the conical nose and the cylindrical part of model 3. It is obvious that the sharpness of the discontinuity on the surface increases the scale of the separation. The necks just before the bases of models 4 and 5 and the extra parts of model 5 also cause flow separation. These circular flow separations have also been observed by the hot-wire measurements in Ref. 21.

On the other hand, as seen from the photographs for $\alpha = 15$ deg, the leeward flow separation produced by the incidence cooperates with the circular flow separations. Thus, the discontinuities in the slope of the body surface make the flow separation and, consequently, the flowfield much more complex relative to those around the simple-type bodies of revolution. The shape of the leeward separation line differs from model to model. It is a continuous curve on models 1 and 2. Along the first half of model 1 it makes a downward concave curve and then on the second half it lies along about the equatorial line of the body. On model 2 it starts from the junction between the hemiellipsoidal nose and cylindrical part, making a wavy curve along the first half part of the cylindrical body and then lies along about the equatorial line. The discontinuities on the surface of the body make the leeward separation discontinuous as seen from the photographs of models 3–5 for $\alpha = 15$ deg. Hence, on the models 4 and 5 the leeward separa-

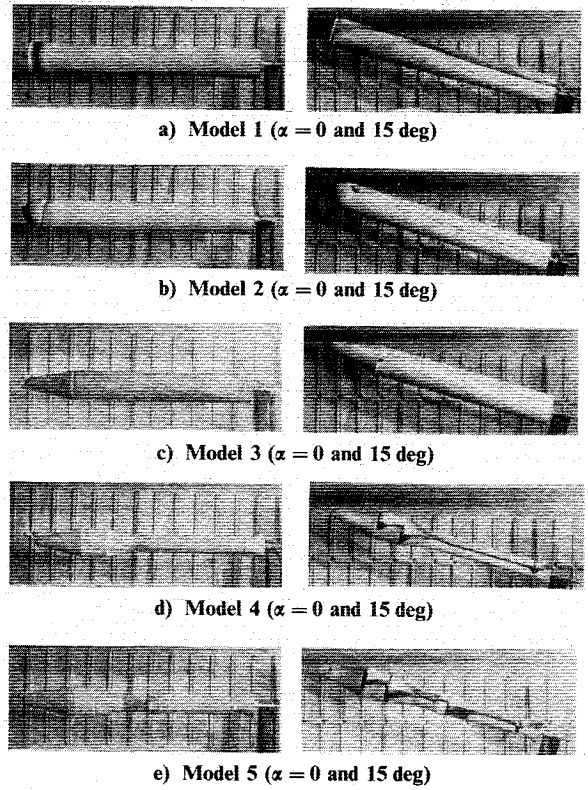

a) Model 1 ($\alpha = 0$ and 15 deg)

b) Model 2 ($\alpha = 0$ and 15 deg)

c) Model 3 ($\alpha = 0$ and 15 deg)

d) Model 4 ($\alpha = 0$ and 15 deg)

e) Model 5 ($\alpha = 0$ and 15 deg)

Fig. 2 Surface flow visualization photographs ($V_\infty = 27$ m/s, scale = 1/10).

tion line takes a form of a step line. In addition, the pairs of vortices exist, one on the right, the other on the left, over the upward of the flat noses and the junctions.

The experimental and theoretical results for the variations for C_N, C_M, C_A, and X_{cp}/l with α are plotted in Figs. 3–6 for all of the five models. The observations obtained from these are the following:

1) Unlike the potential theory, the method based on the crossflow analogy is generally in agreement with the experimental results. This agreement is satisfactory especially for C_N and C_M as seen from Figs. 3 and 4. In fact, it is obvious that the discrepancies for C_N and C_M near zero angle of attack come from the balance. Since the measured values become very small near zero angle of attack, the accuracy of the balance tends to be poor.

As seen from Fig. 5, the agreement between the experimental results and those of Eq. (8) for C_A is better for models 2–4 than that for models 1 and 2. This means that the assumption made with Eq. (8) (that assumes that the axial force is produced only by the axial flowfield) is less valid for blunt-nosed bodies as they are in models 1 and 2.

Although the results of the crossflow method for the location of the center of pressure are better than the results of the potential theory, the discrepancies even between the experimental results and the crossflow method are quite significant, as seen from Fig. 6. The discrepancy is larger near zero angle of attack.

2) The variations of C_N, C_M, and C_A with α are generally nonlinear, while the position of the pressure center (x_{cp}/l) remains almost constant after about 10 deg of incidence.

3) The nose bluntness and the complexity of the geometrical shape increase the drag, as expected.

4) First, the geometrical shape of the body affects not only the drag but also the other aerodynamic force and moment characteristics, such as the variations of C_N and C_M with α, for models 2 and 3 are faster than those for models 4 and 5. This fact may be related to the differences in the flowfield structure from model to model. Although the main parts of models 2 and 3 are the constant-diameter cylinders, models 4 and 5 consist of the cylindrical and conical parts with smaller diameters except a short part on each one. Hence, the width of the wakes of models 4 and 5 would be smaller than those of models 2 and 3. Secondly, as seen from the flow visualization photographs of models 4 and 5 for $\alpha = 15$ deg in Fig. 2, the conical parts on these models move the leeward separation line upward. This would further reduce the widths of the wakes of models 4 and 5 relative to those of models 2 and 3. Consequently, the normal force (or C_N) and the pitching moment (or C_M) would have the higher values for models 2 and 3 than those for models 4 and 5, as seen from Figs. 3 and 4.

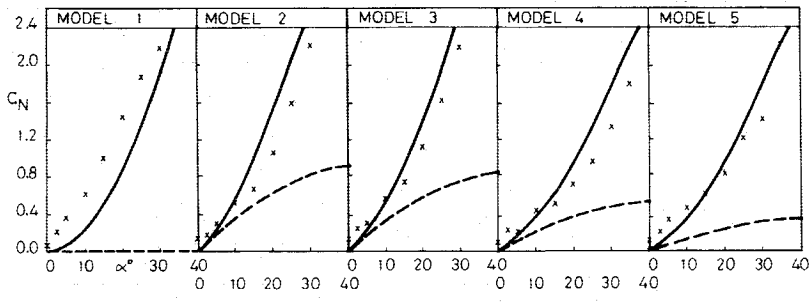

Fig. 3 The variation of C_N with α (x: experimental data, —: method of crossflow analogy, - - - - - -: potential theory).

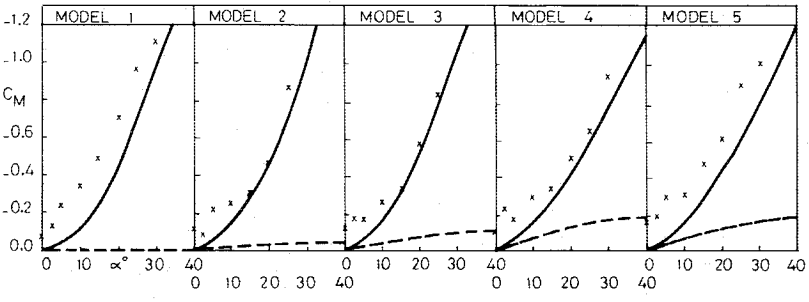

Fig. 4 The variation of C_M with α (x: experimental data, —: method of crossflow analogy, - - - - - -: potential theory).

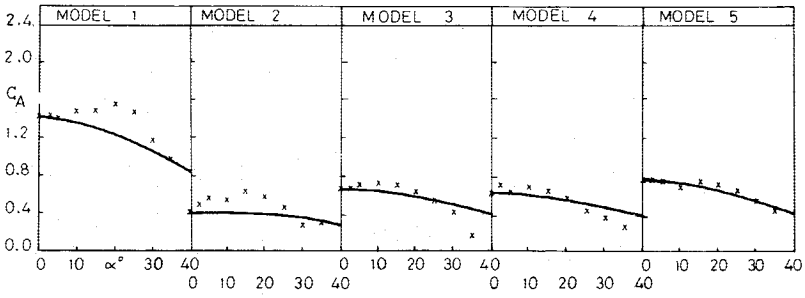

Fig. 5 The variation of C_A with α (x: experimental data, —: $C_A = C_{Do} \cos^2\alpha$).

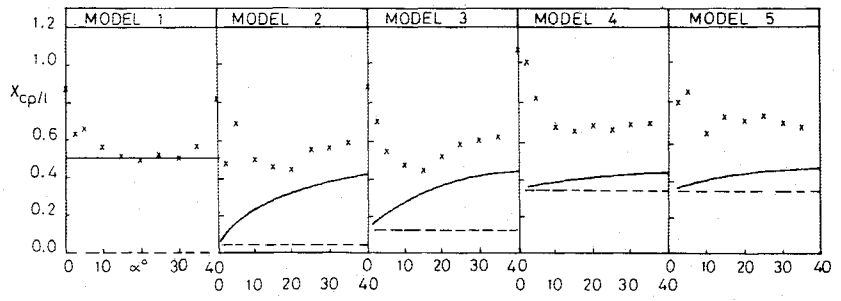

Fig. 6 The variation x_{cp}/l with α (x: experimental data, —: method of crossflow analogy, - - - - -: potential theory).

5) The position of the pressure center depends on the geometrical shape of the body. For instance, $x_{cp}/l \cong 0.5$ for models 1 and 3, while $x_{cp}/l \cong 0.7$ for models 4 and 5, after the angle of incidence increases a few degrees.

Conclusions

The aerodynamics of five complex missile-type bodies of revolution were investigated experimentally and theoretically at a low Mach number ($M_\infty \cong 0.1$). The geometrical forms of the bodies were chosen in such a way as to permit the observation of the effects of the certain geometrical differences on the flowfield and on the aerodynamic characteristics.

The surface flow visualization was made by using the oil method at the angles of attack $\alpha = 0$ and 15 deg. The balance measurements were performed and the potential theory and the method based on the viscous crossflow analogy were applied in order to obtain the variations of C_N, C_M, C_A, and x_{cp}/l with α, experimentally and theoretically, over the range of angle of attack $0 \leqq \alpha \leqq 35$ deg. The comparison was made between the experimental and the theoretical results. The following are the major conclusions of this study:

1) The discontinuities in the slope of the surface of a body of revolution make the flow separation and, consequently, the flowfield very complex. At the zero angle of attack, circular flow separations (or bubbles) exist around the flat nose and the junctions on the body. The bluntness of the flat nose and the sharpness of the junctions increase the scale of the circular separations. If the body of revolution has an angle of attack, the leeward flow separation produced by the incidence cooperates with the circular flow separations. Then, the leeward separation line takes a form of a step line and the pairs of vortices exist over the upward of the flat noses and the junctions.

2) The method based on the viscous crossflow analogy is applicable not only to the simple-type bodies of revolution but also to the complex ones. Although the agreement between the experimental results and the crossflow method is satisfactory for normal force (C_N) and pitching moment (C_M), there are significant discrepancies for the location of the center of pressure (x_{cp}/l). The assumption made in the calculation of the axial force (C_A) (that assumes that the axial force is produced only by the axial flowfield) loses its validity with the bluntness of the body.

3) The complexity of the geometrical shape of a body of revolution affects not only to the drag but also to the other aerodynamic characteristics, such as C_N, C_M, C_A and x_{cp}/l. Since the conical parts of a complex body of revolution move the leeward separation line upward, the width of the wake becomes narrow and then the normal force (or C_N) and the pitching moment (or C_M) become smaller relative to those of a body of revolution of which the main body is a constant-diameter cylinder.

Acknowledgment

The author wishes to acknowledge Professors M. Z. Erim, J. F. Wendt, and Y. Tulunay for their support and the referee of the *AIAA Journal* for his recommendations that improved the paper.

References

[1]Wardlaw, A. B., Jr., "High-Angle-of-Attack Missile Aerodynamics," *Missile Aerodynamics*, AGARD-LS-98, 1979.

[2]Allen, H. J., "Estimation of the Forces and Moments on Inclined Bodies of Revolution of High Fineness Ratio," NACA RM A9126, 1949.

[3]Allen, H. J. and Perkins, E. W., "A Study of Effects of Viscosity on Flow Over Slender Inclined Bodies of Revolution," NACA Rept. 1048, 1951.

[4]Perkins, E. W. and Kuehn, D. M., "Comparison of the Experimental and Theoretical Distributions of Lift on a Slender Inclined Body of Revolution at $M = 2$," NACA TN-3715, 1956.

[5]Perkins, E. W. and Jorgensen, L. H., "Comparison of Experimental and Theoretical Normal-Force Distributions (Including Reynolds Number Effect) on an Ogive-Cylinder Body at Mach Number 1.98," NACA TN-3716, 1956.

[6]Jorgensen, L. H., "Inclined Bodies of Various Cross Sections at Supersonic Speeds," NASA MEMO 10-3-58A, 1958.

[7]Jorgensen, L. H. and Perkins, E. W., "Investigation of Some Wake Vortex Characteristics of an Inclined Ogive-Cylinder Body at Mach Number 2," NACA Rept. 1371, 1958.

[8]Jorgensen, L. H. and Treon, S. L., "Measured and Estimated Aerodynamic Characteristics for a Model of a Rocket Booster at Mach Numbers From 0.6 to 4 and at Angles of Attack From 0° to 180,°" NASA TM-X-580, 1961.

[9]Saffel, B. F., Jr., Howard, M. L., and Brooks, B. N., Jr., "Method for Predicting the Static Aerodynamic Characteristics of Typical Missile Configurations for Angles of Attack to 180 Degrees," Naval Ship Research and Development Center, Rept. 3645, March, 1971.

[10]Jorgensen, L. H., "Prediction of Static Aerodynamic Characteristics for Space-Shuttle-Like and Other Bodies at Angles of Attack from 0° to 180°," NASA TH-D-6996, 1973.

[11]Jorgensen, L. H., "Estimation of Aerodynamics for Slender Bodies Alone and With Lifting Surfaces at α's from 0° to 90°," *AIAA Journal*, Vol. 11, March 1973, pp. 409-412.

[12]Jorgensen, L. H., "A Method for Estimating Static Aerodynamic Characteristics for Slender Bodies of Circular and Noncircular Cross Section Alone and With Lifting Surfaces at Angles of Attack from 0° to 90°," NASA TN-D-7228, 1973.

[13]Jorgensen, L. H., "Prediction of Static Aerodynamic Characteristics for Slender Bodies Alone and With Lifting Surfaces to Very High Angles of Attack," NASA TR-R-474, 1977.

[14]Jorgensen, L. H., "Prediction of Aerodynamic Characteristics for Slender Bodies Alone and With Lifting Surfaces to High Angles of Attack," *High Angle of Attack Aerodynamics*, AGARD-CP-247, 1979.

[15]Lamont, P. J., "Pressures Around an Inclined Ogive Cylinder with Laminar, Transitional, or Turbulent Separation," *AIAA Journal*, Vol. 20, Nov. 1982, pp. 1492-1499.

[16]Yanta, W. J. and Wardlaw, A. B., Jr., "Flowfield about and Forces on Slender Bodies at High Angles of Attack," *AIAA Journal*, Vol. 19, March 1981, pp. 296-302.

[17]Stallings, R. L., Jr., "Reynolds Number Effects on Aerodynamic Characteristics of Large Angles of Attack," *Journal of Spacecraft and Rockets*, Vol. 17, March-April 1980, pp. 129-133.

[18]Przirembel, C. E. G. and Sherda, D. E., "Aerodynamics of Slender Bodies at High Angles of Attack," *Journal of Spacecraft and Rockets*, Vol. 16, Jan.-Feb. 1979, pp. 10-14.

[19]Nielsen, J. N., "Missile Aerodynamics-Past, Present, Future," *Journal of Spacecraft and Rockets*, Vol. 17, May-June 1980, pp. 165-177.

[20]Esch, H., "Bodies," *Missile Aerodynamics*, AGARD-LS-98, 1979.

[21]Atli, V., "Theoretical and Experimental Investigation on the Aerodynamic Characteristics of Some Bodies of Revolution Used in Aeronautics," Ph.D. Thesis, Dept. of Aeronautical Engineering, Istanbul Technical Univ., Turkey, 1984.